Available online at www.sciencedirect.com
ScienceDirect
Electric Power Systems Research 78 (2008) 584–594
ELECTRIC POWER SYSTEMS RESEARCH
www.elsevier.com/locate/epsr

Operating capability of ac EHV mixed lines with overhead and cables links

Roberto Benato *, Antonio Paolucci [1]

Department of Electrical Engineering, University of Padova, Via Gradenigo 6/A, 35131 Padova, Italy

Received 16 May 2006; received in revised form 9 January 2007; accepted 5 May 2007
Available online 21 June 2007

Abstract

A previous paper has been devoted to the operating capability and constraints involved in power transmission of long ac cable links. In this paper the approach has been extended in order to show the transmission performance of some typical mixed configurations with overhead lines (OHL) and cable lines (UGC). These new capability charts are enhanced with other informative parameters, which allow having a wider knowledge of the regimes of a given mixed line. The necessity of limiting the switching overvoltages during composite line energization, by means of shunt reactive compensation, is investigated and criteria for choosing the compensation degree are also presented.

Keywords: XLPE Cable; EHV transmission lines; Underground technology; Shunt compensation

1. Introduction

The enforcing and widening of transmission grid, which are nowadays considered necessary by all parties, are experienced strong difficulties in erecting new overhead lines. This has brought to attention the use of underground transmission technologies: *in primis* the cable lines (UGC). In order to erect a new long link, it could be necessary to have a mix of transmission technologies such as a cascade connection of overhead–cable–overhead lines. In fact, UGCs result more suitable to land constraints and can overcome orographical hindrances. For example, an UGC section allows a HV/EHV link to pass through areas too wide for OHL span such as large rivers or lakes. Very often, the substitution of some OHL spans with UGC is named as "siphon". This configuration may also solve some critical cases due to strongest local oppositions since it drastically reduces the environmental and magnetic impacts and hence it permits the transmission line to pass through or near a protected site (sensible places such as kindergarten) or an urbanised area. It is worth remembering that some important installations of mixed OHL–UGC link have been realised since several years to allow great power flows in town centres.

For the aforementioned reasons, the transmission system operators will have to face more and more the analysis of mixed lines with the aim at achieving the possible performance without jeopardizing either the system safety or the power quality.

2. Mixed lines: OHL–cable–OHL

A rigorous approach to the issue requires to fix, for each section, the specified constraints regarding safety and lifetime of section itself and to research successively the maximum compatible performances of the whole link. A simpler approach can be adopted when the situation is that of Fig. 1 (① OHL–② UGC–③ OHL, with lengths d_1, d_2, and d_3), where the intermediate section is constituted of UGC: in this (very usual) case the constraints expressed by (1) and (2) appear sufficient to satisfy the ampacity not only of the cable but also of OHL ① and ③ :

$$|\underline{I}_H| \leq I_c \tag{1}$$

$$|\underline{I}_K| \leq I_c \tag{2}$$

$$|\underline{U}_{oS}| = U_{oc}. \tag{3}$$

The value of I_c represents the current limit which must not exceed the ampacity of cable section ② : it is sufficient that I_c (imposed at H and K) is little lower than the ampacity of OHL ① and ③ to obtain (as it will have to be systematically verified) allowable current levels also at S and R. Ultimately, the relation (3) fixes the voltage at S, similarly

* Corresponding author. Tel.: +39 049 8277532; fax: +39 049 8277599.
E-mail address: roberto.benato@unipd.it (R. Benato).
[1] Tel.: +39 049 8277516; fax: +39 049 8277599.

0378-7796/$ – see front matter © 2007 Elsevier B.V. All rights reserved.
doi:10.1016/j.epsr.2007.05.002

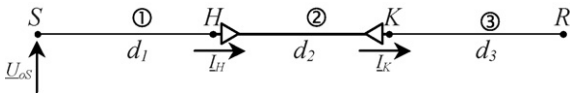

Fig. 1. Typical sketch of mixed line.

Table 1
Positive-sequence parameters of OHL (for typical installation)

Overhead #	①, ③
Voltage level (kV)	400
Sub-conductor	3 sub-cond. ACSR Ø 31.5 mm spac. = 40 cm
Resistance at 75 °C (50 Hz), r (mΩ/km)	23.10
Per unit length series inductance, l (mH/km)	0.858
Per unit length shunt leakance (50 Hz), g (nS/km)	10
Per unit length capacitance, c (μF/km)	0.0133
Ampacity, I_a (A)	
Cold months	2955
Warm months	2220

to the settlement already adopted in ref. [1]. In the following investigations, where $U_m = 420$ kV, it has retained the level $U_{oc} = 230\,\text{kV} = 95\%U_m/\sqrt{3}$.

In this paper, a complete three-phase symmetry of the lines has been assumed: this requires phase transpositions for OHL and for cable line also the cross-bonding arrangement and allows the use of classical transmission equations based on positive sequence parameters (see Table 1 for OHL and Table 2 for single-circuit UGC) and of relevant matrices (see Appendix A).

This is a useful guide also for unbalance systems provided that a slightly conservative choice of I_c and U_{oc} is made. Successively, a deep insight can be performed by means of multi-conductor study [2,3]. This approach takes into account, beyond the structural dissymmetry of phase conductors, also that due to the presence of the ground wires of OHL and shields of UGC.

In this paper, for OHL a typical 400 kV line of Italian grid (equipped with bundles of three sub-conductors) has been considered and for UGC ② a 400 kV double-circuit consisting of single-pole 2500 mm^2 copper conductor XLPE cables.

Once considered the values of ampacity for OHL (foreseen by Italian Standard; see Table 1), the levels I_c (during cold months) = 2800 A and I_c (during warm months) = 2100 A have been assumed in (1) and (2), as specified in each case studies. These choices do not seem to be excessively redundant for section ② with $I_a = 2 \times 1788$ A as shown in Table 2 ($(2 \times 1788)/2800) = 1.28$ during cold months and $(2 \times 1788)/2100) = 1.70$ during warm months) because it seems a conservative installation criterion to have a good power reserve in case of a circuit failure. The analysis of link between nodes S and R, not inserted in the real context of a given electric network, constitutes a preliminary assessment and a useful guide for further network studies (among which the power flow and network simulations are indispensable). In analogy with [1], the regime of this mixed line can be achieved by means of a first analysis ($\underline{U}_{oS}$ and $|\underline{I}_K|$ constrained) and a successively second one ($\underline{U}_{oS}$ and $|\underline{I}_H|$ constrained), with the aim at individuating the regimes that respect also the ampacity at S and R.

Table 2
Positive-sequence parameters of single-circuit UGC (for typical installation)

Cable #	②
Voltage level (kV)	400
Cross-section (mm^2)	2500 Cu
Apparent resistance at 90 °C (50 Hz), r (mΩ/km)	13.3
Per unit length inductance, l (mH/km)	0.576
Per unit length shunt leakance (50 Hz) with $\tan\delta = 0.0007$, g (nS/km)	51.5
Per unit length, capacitance with, $\varepsilon_r = 2.3$ (μF/km)	0.234
Ampacity, I_a (A)	1788

3. First analysis

Once fixed at node K the current phasor $\underline{I}_K = I_c\angle 0$ (on the real axis), and imposed at node S the following phasor

$$U_{oS} = 230\,\text{kV}\angle\delta \quad (\delta = 0 \div 2\pi)$$

a set of regimes of the entire line is univocally achieved, among which only those respecting the limit I_c at node H must be individuated. In particular the relations (4)–(9′), (which hold the matrices shown in Appendix A) show the subsequent formal passages, which give the Eq. (10), deriving from (9′). The expression (10) can be interpreted by the phasorial diagram of Fig. 2 (with some modified proportions for graphical purposes) which, by means of the relations shown in the same figure, yields the problem solution: for δ ranging between δ_1 and δ_2 (evaluated by means of (11) and (12)), the voltage phasor $\underline{U}_{oS}(\delta)$ determines in this first analysis all the current phasors $\underline{I}_H$ (e.g. OL_1, OL_3, OL_4, OL_2) having magnitudes within the limit I_c according to (2) as long as the magnitudes of phasors a, b, c are compatible with the triangular configuration. In particular, the phasors OL_1 and OL_2, (the former leading and the latter lagging with respect to I_K) regard currents $\underline{I}_H$ with the same magnitude of $I_c = |\underline{I}_K|$.

$$\begin{bmatrix} \underline{U}_{oS} \\ \underline{I}_S \end{bmatrix} = \begin{bmatrix} \underline{A}_{12} & \underline{B}_{12} \\ \underline{C}_{12} & \underline{D}_{12} \end{bmatrix} \begin{bmatrix} \underline{U}_{oK} \\ \underline{I}_K \end{bmatrix} \quad \underline{\boldsymbol{v}}_{SS(K)} \quad \underline{\boldsymbol{M}}_{12} \quad \underline{\boldsymbol{v}}_K \tag{4}$$

$$\begin{bmatrix} \underline{U}_{oK} \\ \underline{I}_K \end{bmatrix} = \begin{bmatrix} \underline{D}_{12} & -\underline{B}_{12} \\ -\underline{C}_{12} & \underline{A}_{12} \end{bmatrix} \begin{bmatrix} \underline{U}_{oS} \\ \underline{I}_S \end{bmatrix} \quad \underline{\boldsymbol{v}}_K \quad \underline{\boldsymbol{M}}_{12}^{-1} \quad \underline{\boldsymbol{v}}_{SS(K)} \tag{5}$$

$$\begin{bmatrix} \underline{U}_{oS} \\ \underline{I}_K \end{bmatrix} = \begin{bmatrix} 1 & 0 \\ -\underline{C}_{12} & \underline{A}_{12} \end{bmatrix} \begin{bmatrix} \underline{U}_{oS} \\ \underline{I}_S \end{bmatrix} \quad \underline{\boldsymbol{v}}_{SK} \quad \underline{\boldsymbol{v}}_{SS(K)} \tag{6}$$

$$N_{Sl} = \begin{bmatrix} 1 & 0 \\ -\underline{C}_{12} & \underline{A}_{12} \end{bmatrix}^{-1} \tag{7}$$

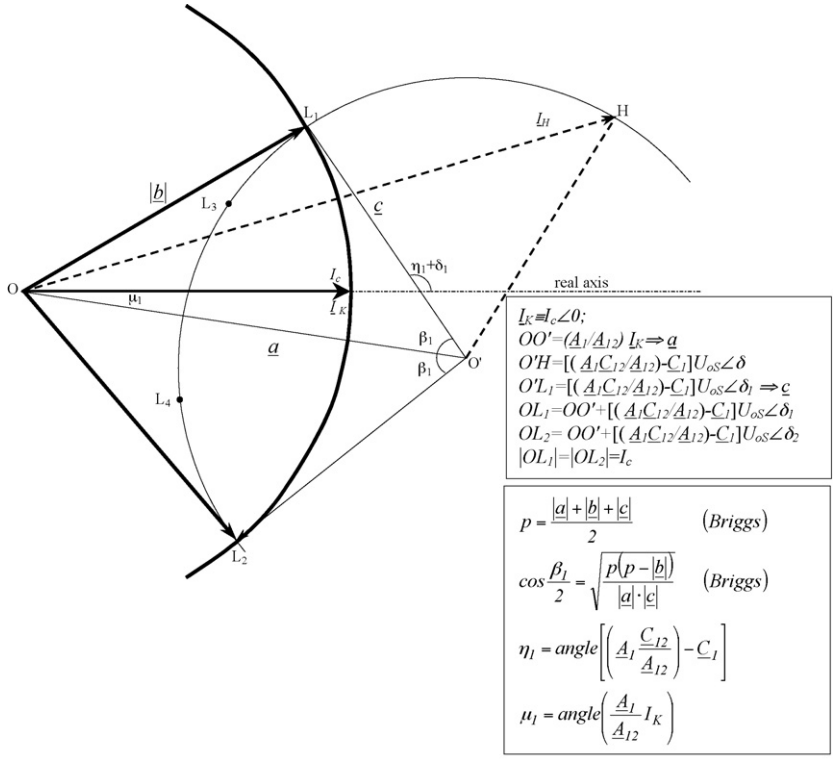

Fig. 2. Phasorial diagram of the Eq. (10).

$$\begin{bmatrix} \underline{U}_{oS} \\ \underline{I}_S \end{bmatrix} = \begin{bmatrix} 1 & 0 \\ \dfrac{\underline{C}_{12}}{\underline{A}_{12}} & \dfrac{1}{\underline{A}_{12}} \end{bmatrix} \begin{bmatrix} \underline{U}_{oS} \\ \underline{I}_K \end{bmatrix} \qquad \underline{\boldsymbol{v}}_{SS(K)} = \underline{\boldsymbol{N}}_{S1}\,\underline{\boldsymbol{v}}_{SK} \tag{8}$$

$$\underline{\boldsymbol{v}}_{HH(K)} = \underline{\boldsymbol{M}}_1^{-1}\,\underline{\boldsymbol{v}}_{SS(K)} \tag{9}$$

$$\begin{bmatrix} \underline{U}_{oH} \\ \underline{I}_H \end{bmatrix} = \begin{bmatrix} \underline{D}_1 & -\underline{B}_1 \\ -\underline{C}_1 & \underline{A}_1 \end{bmatrix} \begin{bmatrix} 1 & 0 \\ \dfrac{\underline{C}_{12}}{\underline{A}_{12}} & \dfrac{1}{\underline{A}_{12}} \end{bmatrix} \begin{bmatrix} \underline{U}_{oS} \\ \underline{I}_K \end{bmatrix} \qquad \underline{\boldsymbol{v}}_{HH(K)} = \underline{\boldsymbol{M}}_1^{-1}\,\underline{\boldsymbol{N}}_{S1}\,\underline{\boldsymbol{v}}_{SK} \tag{9'}$$

: imposed phasors

$$\underline{I}_H = \left(-\underline{C}_1 + \frac{\underline{A}_1 \cdot \underline{C}_{12}}{\underline{A}_{12}}\right) \cdot \underline{U}_{oS} + \frac{\underline{A}_1}{\underline{A}_{12}} \cdot \underline{I}_K \tag{10}$$

$$\delta_1 = \pi - \beta_1 - \eta_1 + \mu_1 \tag{11}$$

$$\delta_2 = \delta_1 + 2\beta_1 \tag{12}$$

4. Second analysis

In an analogue way, once fixed at node H the current phasor $\underline{I}_H = I_c\angle 0$ (on the real axis), and imposed at node S the following phasor

$$\underline{U}_{oS} = 230\,\text{kV}\angle\vartheta, \quad (\vartheta = 0 \div 2\pi),$$

another set of regimes can be achieved among which only those respecting the limit I_c at node K are of interest.

The relations from (13) to (18′) show the subsequent formal passages, which give rise to Eq. (19). It can be interpreted by the phasorial diagram of Fig. 3: by means of the relations shown in the same figure, it is possible to see that, for ϑ ranging between ϑ'' and ϑ' (evaluated by means of (20) and (21)), the voltage phasor $\underline{U}_{oS}(\vartheta)$ determines in this second analysis all the current phasors $\underline{I}_K$ (e.g. OL'', OL''', OL'''', OL') with magnitudes within the limit I_c, according to (1).

$$\begin{bmatrix} \underline{U}_{oS} \\ \underline{I}_S \end{bmatrix} = \begin{bmatrix} \underline{A}_1 & \underline{B}_1 \\ \underline{C}_1 & \underline{D}_1 \end{bmatrix} \begin{bmatrix} \underline{U}_{oH} \\ \underline{I}_H \end{bmatrix} \qquad \underline{\boldsymbol{v}}_{SS(H)} = \underline{\boldsymbol{M}}_1\,\underline{\boldsymbol{v}}_H \tag{13}$$

$$\begin{bmatrix} \underline{U}_{oH} \\ \underline{I}_H \end{bmatrix} = \begin{bmatrix} \underline{D}_1 & -\underline{B}_1 \\ -\underline{C}_1 & \underline{A}_1 \end{bmatrix} \begin{bmatrix} \underline{U}_{oS} \\ \underline{I}_S \end{bmatrix} \qquad \underline{\boldsymbol{v}}_H = \underline{\boldsymbol{M}}_1^{-1}\,\underline{\boldsymbol{v}}_{SS(H)} \tag{14}$$

$$\begin{bmatrix} \underline{U}_{oS} \\ \underline{I}_H \end{bmatrix} = \begin{bmatrix} 1 & 0 \\ -\underline{C}_1 & \underline{A}_1 \end{bmatrix} \begin{bmatrix} \underline{U}_{oS} \\ \underline{I}_S \end{bmatrix} \qquad \underline{\boldsymbol{v}}_{SH} = \underline{\boldsymbol{N}}_{S2}\,\underline{\boldsymbol{v}}_{SS(H)} \tag{15}$$

$$\underline{\boldsymbol{N}}_{S2} = \begin{bmatrix} 1 & 0 \\ -\underline{C}_1 & \underline{A}_1 \end{bmatrix}^{-1} \tag{16}$$

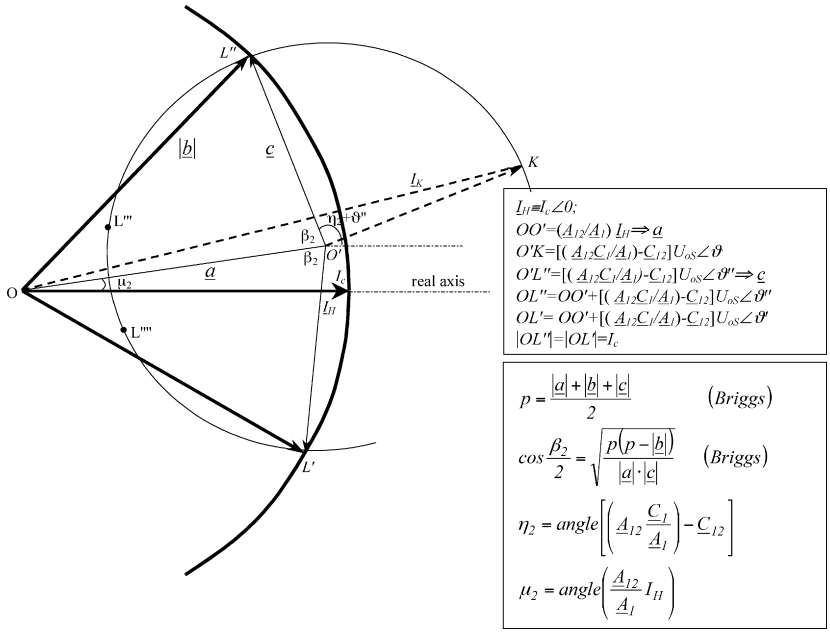

Fig. 3. Phasorial diagram of the Eq. (19).

$$\begin{bmatrix}\underline{U}_{oS}\\ \underline{I}_S\end{bmatrix} = \begin{bmatrix}1 & 0\\ \frac{\underline{C}_1}{\underline{A}_1} & \frac{1}{\underline{A}_1}\end{bmatrix}\begin{bmatrix}\underline{U}_{oS}\\ \underline{I}_H\end{bmatrix} \qquad \underline{\boldsymbol{v}}_{SS(H)} = \underline{\boldsymbol{N}}_{S2}\cdot\underline{\boldsymbol{v}}_{SH} \tag{17}$$

$$\underline{\boldsymbol{v}}_{KK(H)} = \underline{\boldsymbol{M}}_{12}^{-1}\cdot\underline{\boldsymbol{v}}_{SS(H)} \tag{18}$$

$$\begin{bmatrix}\underline{U}_{oK}\\ \underline{I}_K\end{bmatrix} = \begin{bmatrix}\underline{D}_{12} & -\underline{B}_{12}\\ -\underline{C}_{12} & \underline{A}_{12}\end{bmatrix}\begin{bmatrix}1 & 0\\ \frac{\underline{C}_1}{\underline{A}_1} & \frac{1}{\underline{A}_1}\end{bmatrix}\begin{bmatrix}\underline{U}_{oS}\\ \underline{I}_H\end{bmatrix} \qquad \underline{\boldsymbol{v}}_{KK(H)} = \underline{\boldsymbol{M}}_{12}^{-1}\cdot\underline{\boldsymbol{N}}_{S2}\cdot\underline{\boldsymbol{v}}_{SH} \tag{18′}$$

$$\underline{I}_K = \left(-\underline{C}_{12} + \underline{A}_{12}\cdot\frac{\underline{C}_1}{\underline{A}_1}\right)\cdot\underline{U}_{oS} + \frac{\underline{A}_{12}}{\underline{A}_1}\cdot\underline{I}_H \tag{19}$$

In particular, the phasors OL'' and OL' reproduce again the same relations of magnitude and angle (with respect to I_H) detectable in the first analysis for OL_1 and OL_2.

$$\vartheta'' = \pi - \beta_2 - \eta_2 + \mu_2 \tag{20}$$

$$\vartheta' = \vartheta'' + 2\beta_2 \tag{21}$$

It is worth noting that the double-circuit UGC in section ② requires (see Section 6), due to its great capacitive susceptance, almost always a suitable degree of compensation ξ_{sh} which, modifying the elements of matrix $\underline{\boldsymbol{M}}_2$ (and hence of $\underline{\boldsymbol{M}}_{12}$, $\underline{\boldsymbol{M}}_{123}$), affects all the line regimes. The hypothesis of uniformly distributed shunt compensation has been adopted also in this paper as in [1]: it allows determining (notwithstanding the idealized approach) the suitable power system solutions.

5. The capability charts

The procedures presented in the first and second analysis allow individuating, for a given mixed line, all the regimes at power frequency compatible with the constraints (1)–(3), yielding for each regime the vector (composed of voltage and current phasors) at each node. Therefore, it becomes particularly interesting the complex power at end nodes S and R. In order to evaluate the complex power $\underline{S}_S$ at node S the elements of vectors $\underline{\boldsymbol{v}}_{SS(K)}$ in (8) and $\underline{\boldsymbol{v}}_{SS(H)}$ in (17) must be used, whereas for complex power $\underline{S}_R$ at node R the elements of vectors $\underline{\boldsymbol{v}}_{RR(K)}$ in (22) and $\underline{\boldsymbol{v}}_{RR(H)}$ in (23) must be adopted.

It is worth noting that the relations (22) and (23) as well as (8) and (17) are useful to verify (as already discussed in Section 2) the respect of ampacity at R and S for OHLs.

$$\begin{bmatrix}\underline{U}_{oR}\\ \underline{I}_R\end{bmatrix} = \begin{bmatrix}\underline{D}_{123} & -\underline{B}_{123}\\ -\underline{C}_{123} & \underline{A}_{123}\end{bmatrix}\begin{bmatrix}1 & 0\\ \frac{\underline{C}_{12}}{\underline{A}_{12}} & \frac{1}{\underline{A}_{12}}\end{bmatrix}\begin{bmatrix}\underline{U}_{oS}\\ \underline{I}_K\end{bmatrix} \qquad \underline{\boldsymbol{v}}_{RR(K)} = \underbrace{\underline{\boldsymbol{M}}_{123}^{-1}\cdot\underline{\boldsymbol{N}}_{S1}}_{\underline{\boldsymbol{N}}_{R1}}\cdot\underline{\boldsymbol{v}}_{SK}$$

$$\begin{bmatrix}\underline{U}_{oR}\\ \underline{I}_R\end{bmatrix} = \begin{bmatrix}\underline{D}_{123} & -\underline{B}_{123}\\ -\underline{C}_{123} & \underline{A}_{123}\end{bmatrix}\begin{bmatrix}1 & 0\\ \frac{\underline{C}_1}{\underline{A}_1} & \frac{1}{\underline{A}_1}\end{bmatrix}\begin{bmatrix}\underline{U}_{oS}\\ \underline{I}_H\end{bmatrix} \qquad \underline{\boldsymbol{v}}_{RR(H)} = \underbrace{\underline{\boldsymbol{M}}_{123}^{-1}\cdot\underline{\boldsymbol{N}}_{S2}}_{\underline{\boldsymbol{N}}_{R2}}\cdot\underline{\boldsymbol{v}}_{SH} \tag{22, 23}$$

The respect of ampacity along the UGC length appears (in any case-study) assured *a priori*, since the ratios between ampacity and I_c are 1.28 (cold months) and 1.7 (warm months). If the

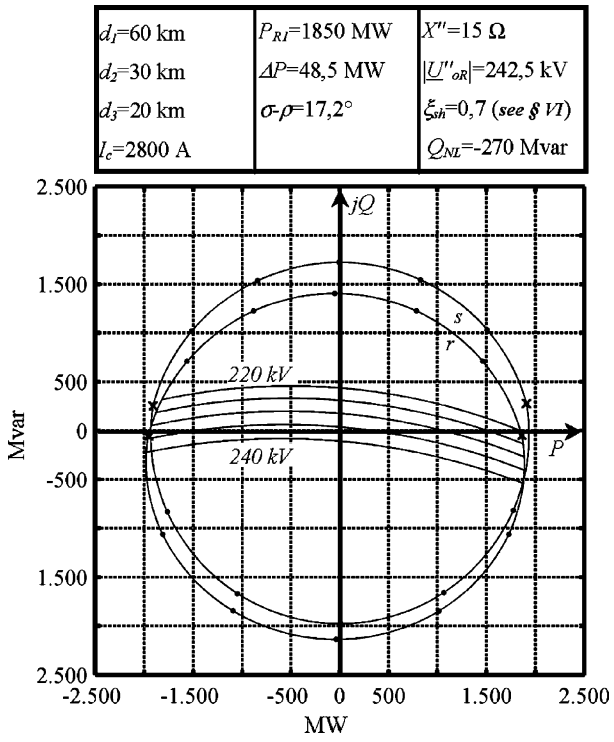

Fig. 4. A first example of capability chart.

ratio is less conservative, it is advisable to make some controls by means of (A4′) and (A4″) (with similar behaviours as in [1]). Hence the outlines can be drawn (see the example of Fig. 4): the outline s bounds the "sending-end power area" and the outline r the "receiving-end power area", respecting the fixed constraints. It can be ascertained (see Section 8) that they are composed of arcs of circumference and ellipse, analytically inferable.

At regular steps, it is possible to mark the complex power $\underline{S}_S$ and $\underline{S}_R$ with couple of points upon the outlines s and r: their correspondence is easily detectable by the mutual proximity (see Fig. 4). The difference $\underline{S}_S - \underline{S}_R$ views with the real part the active transmission power losses and with the imaginary part the reactive power demand by the composite system (including reactive compensation, if any).

The couples of points marked with × represent the particular regimes (see Sections 3 and 4) characterized by $|\underline{I}_K| \equiv |\underline{I}_H| \equiv I_c$. These capability charts for mixed link give (as already seen for only cable lines in [1]) immediate visual information on power flow performances. Moreover, as shown in the first example of Fig. 4, each capability chart can be enhanced with the following transmission parameters (very useful to detail even more the power quality):

- Maximum receiving-end power P_{R1} at $\cos\varphi = 1$ with the corresponding power losses ΔP and phase angle σ–ρ between $\underline{U}_{oS}$ and $\underline{U}_{oR}$;
- Voltage levels at R;
- Degree ξ_{sh} of shunt compensation (for section ②) necessary to limit at $U_m/\sqrt{3}$ the subtransient overvoltages U''_{oR} in a typical case of no-load line energisation (see Section 6);
- Capacitive reactive power Q_{NL} absorbed in S by the mixed link at no load in R in steady-state regime with chosen ξ_{sh};(meaning for the breaking tests)

5.1. P_{R1}, ΔP and σ–ρ

The maximum active receiving-end power P_{R1} (at $\cos\varphi = 1$) is generally detectable in the around of δ_1 in the first analysis or in the around of ϑ' in the second analysis and appears very meaningful in order to evaluate the more interesting performances and power flows of the mixed line, together with the power losses ΔP and the angle σ–ρ.

5.2. Phase voltage levels at R

The voltage levels at node R plays a key role in the network service and can be directly visualised in the "receiving-end power area" by means of phase voltage curves parameterized with $|\underline{U}_{oR}|$ constant, implementing the well-known expression of receiving-end power

$$\underline{S}_R = 3\underline{U}_{oR}\left[\frac{(\underline{U}_{oS} - \underline{A}_{123}\underline{U}_{oR})}{B_{123}}\right]^*. \tag{23′}$$

Once fixed $\underline{U}_{oS} = 230\,\text{kV}\angle\sigma$ and by setting $\underline{U}_{oR}\angle\rho$ (e.g. with magnitudes 220, 225, 230, 235, 240 kV) it is possible to give suitable σ–ρ values such to determine complex power $\underline{S}_R$ in the "receiving-end area".

In such a way, it can be clearly singled out the regimes which are not acceptable owing to excessively high or low voltage levels at R (even if compatible with limit I_c): for example, heavy reactive power flows or active ones on long runs. In particular the voltage curve intersecting the origin also points out the voltage in receiving-end at no-load regime ($P_R + \text{j}Q_R \equiv 0$), when $|\underline{U}_{oS}| = 230\,\text{kV}$.

6. No load energization

The per unit-length capacitive susceptance of UCG (a double-circuit in the case-study) is worth about 35 times that of OHL and can require (depending upon d_2 length) strong capacitive power: this reactive susceptance affects sensibly the capability charts and plays a key role on the transient and steady-state regimes of the composite line at no-load. A rough estimation brings to compute, for the double-circuit UGC (see Table 2), the heavy capacitive power $Q_C \approx 2(3U_o^2\omega c) = 23\,\text{Mvar/km}$ at 50 Hz and 28 Mvar/km at 60 Hz: it becomes foreseeable that shunt compensations are almost always necessary both for good effects on capability charts and for the switching-on of no-load line. In fact, in the network operation, a very frequently recurring event of greatest concern is the energization of a no-load line since it is always necessary to prepare the operating structure of the grid. The sketch of Fig. 5 shows the switch-on of the circuit breaker in S in order to energize the mixed line and serves as a first approximated but meaningful approach devoted to highlight the limit conditions for line energization at no-load. The supply in S can be modelled as an equivalent generator (as seen at node

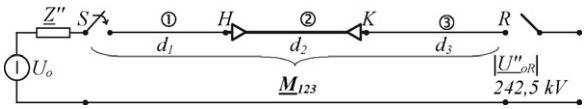

Fig. 5. Typical sketch of mixed line at no-load at *R*.

S belonging to a given network) which is characterized by its electromotive force U_o (supposed to be equal to 230 kV) and the short-circuit subtransient impedance $\underline{Z}''$ (for simplicity purely inductive $\underline{Z}'' = \mathrm{j}X''$).

The no-load power frequency subtransient voltage $\underline{U}''_{oR}$ at *R*, due to the closing at *S*, is completely defined by the following formulae:

$$\underline{U}''_{oS} = \left(\frac{U_o}{\underline{Z}'' + (\underline{A}_{123}/\underline{C}_{123})}\right) \cdot \frac{\underline{A}_{123}}{\underline{C}_{123}} \tag{24}$$

$$\underline{U}''_{oR} = \frac{\underline{U}''_{oS}}{\underline{A}_{123}} \tag{25}$$

$$\underline{U}''_{oR} = \frac{U_o}{\underline{A}_{123} + \underline{Z}'' \cdot \underline{C}_{123}} \tag{26}$$

being $\underline{A}_{123}/\underline{C}_{123}$ the impedance (almost completely capacitive) as seen from *S* with *R* at no-load, and expressing with (25) the Ferranti's effect.

With regard to $\underline{Z}'' = \mathrm{j}X''$ evaluation, it is possible to refer firstly to the subtransient impedance U_o/I''_{sc} (from network studies). The values of subtransient short circuit current I''_{sc} (three-phase at *S*) in *EHV* networks can be foreseen in the range 10–50 kA, so that X'' corresponds to 23–4.6 Ω.

In order to respect the standard switching levels (e.g. 1050 kV) with a conservative margin, it seems advisable that the phasor $\underline{U}''_{oR}$ does not exceed the magnitude $U_m/\sqrt{3} = 242.5$ kV.

The necessary value of ξ_{sh} to achieve $|\underline{U}''_{oR}| = 242,5$ kV in (26) can be easily computed with automatic iterations once fixed the parameters d_1, d_2, d_3, X'', U_o.

Since the target depends upon numerous parameters, the Figs. 6 and 7 report only some possible situations that are very useful to frame the phenomenon.

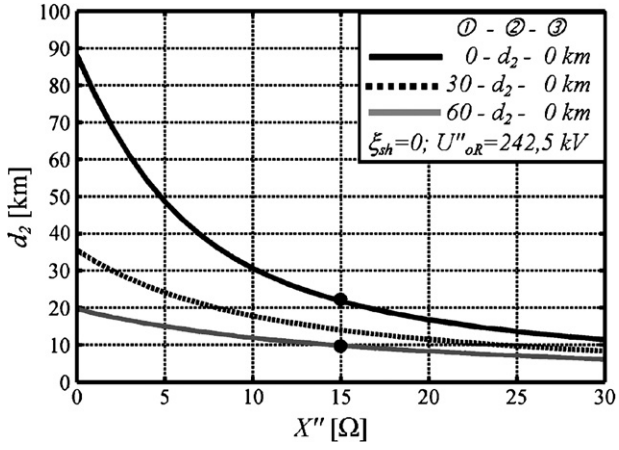

Fig. 6. Examples of limit length d_2 of UGC ($\xi_{sh} = 0$) as function of subtransient short-circuit reactance X''.

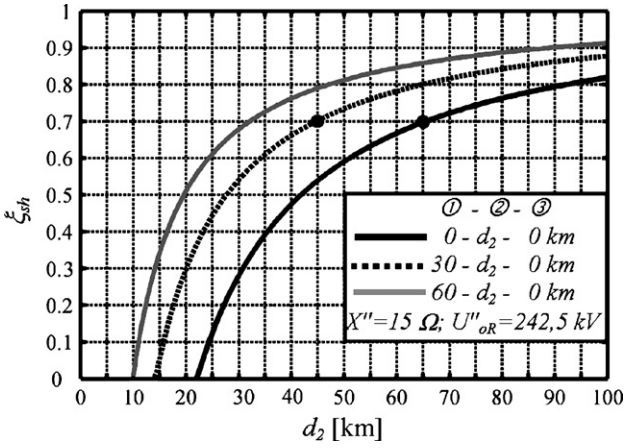

Fig. 7. Examples of compensation degree ξ_{sh} as function of UGC length d_2.

The curves of Fig. 6 show, for example, that with $\xi_{sh} = 0$ and $X'' = 15\ \Omega$ the length d_2 of UGC cannot exceed 22 km if $d_1 = 0$ and even 10 km if $d_1 = 60$ km.

The curves of Fig. 7 (computed for $X'' = 15\ \Omega$) show for example how (set $d_3 = 0$) the section UGC with $\xi_{sh} = 0.7$ can reach $d_2 = 65$ km if $d_1 = 0$ km or $d_2 = 45$ km if $d_1 = 30$ km.

It is worth noting that the OHL ① chiefly introduces (at 50 Hz) a longitudinal reactance (≅0.27 Ω/km) which "increases" the short-circuit reactance with all the obvious consequences (i.e. reduction of maximum UGC length, increase of compensation degree). Once the value of ξ_{sh} has been computed by means of (26), it is useful to assess through (27) the power (almost entirely capacitive one) absorbed by mixed line (at no-load) supplied at node *S* with steady-state voltage U_o (e.g. 230 kV) in the hypothesis that, after the switching transients, it is restored.

$$S_{NL} = 3 \cdot U_o^2 \cdot \frac{\underline{C}^*_{123}}{\underline{A}^*_{123}} \cong Q_{NL}. \tag{27}$$

This value is important for the corresponding breaking test.

Figs. 8 and 9 consider examples where $d_3 > 0$. It is evident that the energization of no-load mixed line from the node *R* must be evaluated by considering the lengths of three section in the right order: for example, if the order from *S* to *R* of the lengths d_1,

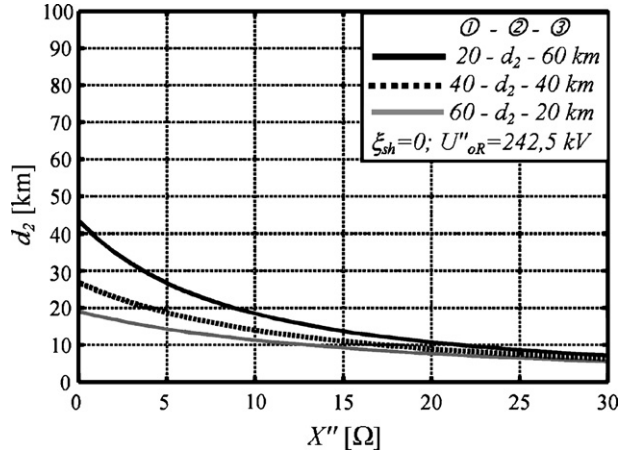

Fig. 8. Examples of limit length d_2 of UGC ($\xi_{sh} = 0$) as function of subtransient short-circuit reactance X''.

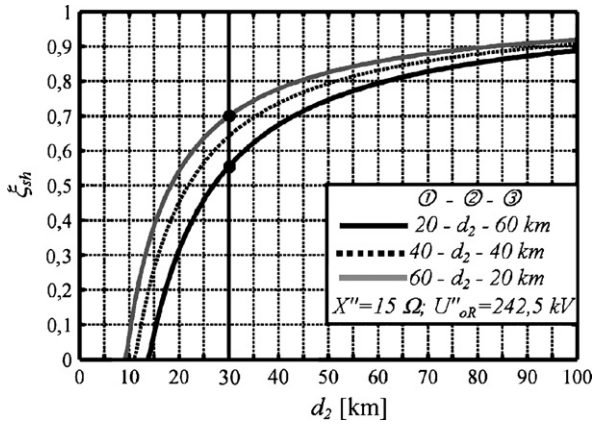

Fig. 9. Examples of compensation degree ξ_{sh} as function of UGC length d_2.

d_2, d_3 is 60, 30, 20 km, when the energization from S is assessed the grey curve in Fig. 9 must be considered, whereas the dark curve with energization from R. If the equivalent generators at both ends were equal (same $U_o = 230$ kV and same $X'' = 15\ \Omega$) it would be better the energization from R, which requires a lower compensation degree. On the other hand, it appears very likely that the receiving-end is a very weak node (very high X'') so that it results less suitable than S for the energization of no-load line: the detection of "best-end" switching [4] is mentioned by CEGB as effective experienced practices in network operations. It is trivial to remember the possibility for the TSO of energising the line with voltage temporarily reduced. These first meaningful considerations on the subtransient regimes must be followed by an in-depth analysis of power flows and network simulations in order to fix the suitable compensation degree for UGC section.

As already stated, the hypothesis of uniformly distributed shunt compensation has been adopted also in this paper as in [1]: it has been throughout verified that both the capability charts and the subtransient voltage due to line energization remain almost unchanged by applying (with the same ξ_{sh}) lumped shunt compensations (see suitable matrices $\underline{\boldsymbol{M}}_{\xi}$ in Appendix A) on length intervals not greater than 15–20 km. Some attention must be paid for the precise location of the limit I_c at H and K (in the matrix cascade).

7. The use of capability charts as a guide

The example of Fig. 4 already gives an idea of the utility of the capability charts for transmission system operators. It is worth remembering that the value of ξ_{sh} (evaluated after Section 6), is not only fundamental for a good line energization but also determines satisfactory steady-state regimes. Moreover the set of curves parameterized with phase voltages 220–240 kV highlights immediately how a good voltage level at R constitutes a further limiting constraint (chiefly for reactive power) within the capability charts for $I_c = 2800$ A. Also the values of maximum transmissible active power P_{R1} together with the power losses ΔP and the compensation degree ξ_{sh} are very useful for economic evaluations: in particular, the compensation degree

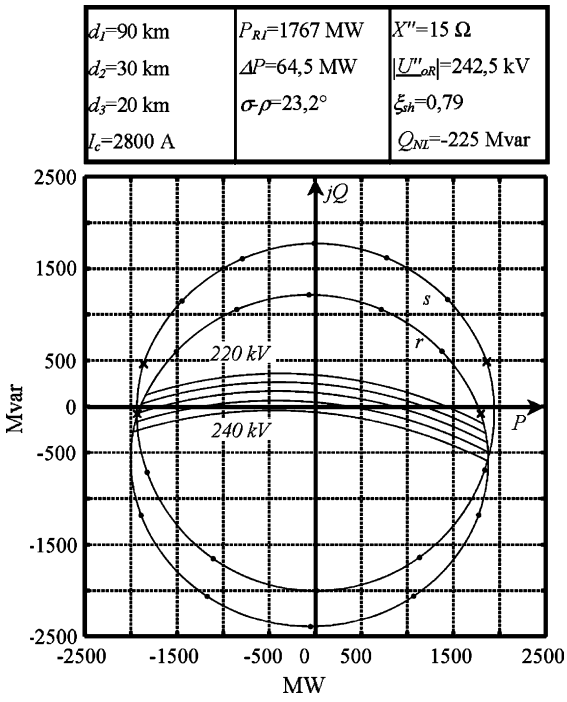

Fig. 10. Capability chart of specified mixed line.

constitutes a direct reference to the installation cost of shunt reactors in section ② . The no-load steady-state reactive power $Q_{NL} = -270$ Mvar does not appear problematic. Fig. 10 highlights how the increased overall length of mixed line (90, 30, 20 km) yields unacceptable voltage drops unless the node R has not strongly capacitive load. So it is possible to understand that when the mixed line length increases, the criterion of voltage drops and power losses becomes paramount: in correspondence of the power flow $P_{R1} = 1767$ MW is $|\underline{U}_{oR}| = 210$ kV (as easily graphically inferable) and a ratio $\Delta P/P_{R1} = 3.65\%$ rather high.

Fig. 11 clearly shows how choosing a current limit of 2100 A (just below OHL warm month ampacity) gives regimes more rational than those of Fig. 10.

Both Figs. 12 and 13, which can represent some examples of mixed line for penetration in town centres ($d_3 = 0$), show how the decreased overall length with reference to the foregoing case (110 km rather than 140 km) allows (in cold months) a higher chosen current limit (2500 A) and good voltage levels at R.

The comparison between Figs. 12 and 14 underlines the reduction of capability charts due to current limit (2100 A) and the subsequent better voltage levels at R. Figs. 15 and 16 also appear very meaningful because they deal with cases where the line between S and R is entirely constituted by double-circuit UGC of 60 km (having set $d_1 = 0$, $d_2 = 60$, $d_3 = 0$).

Fig. 15 shows the excellent performance ($P_{R1} = 2385$ MW) of 60 km compensated double-circuit cable (due to its very high ampacity limit 3500 A) with good voltage levels because of its low longitudinal impedance.

The problems of uncompensated UGC (with the same length) in Fig. 16 are both the highest reactive power Q_{NL} (−1423 Mvar) and the subtransient voltage level U''_{oR} (272 kV) during energization.

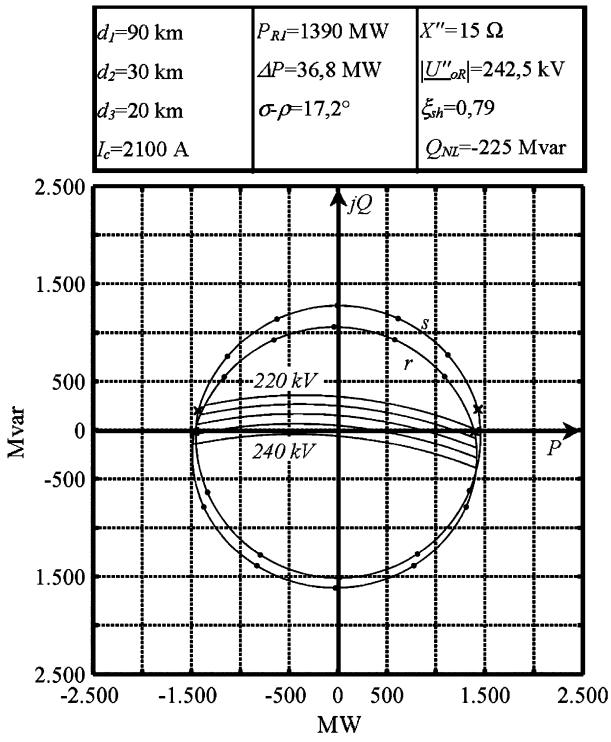

Fig. 11. Capability chart of specified mixed line.

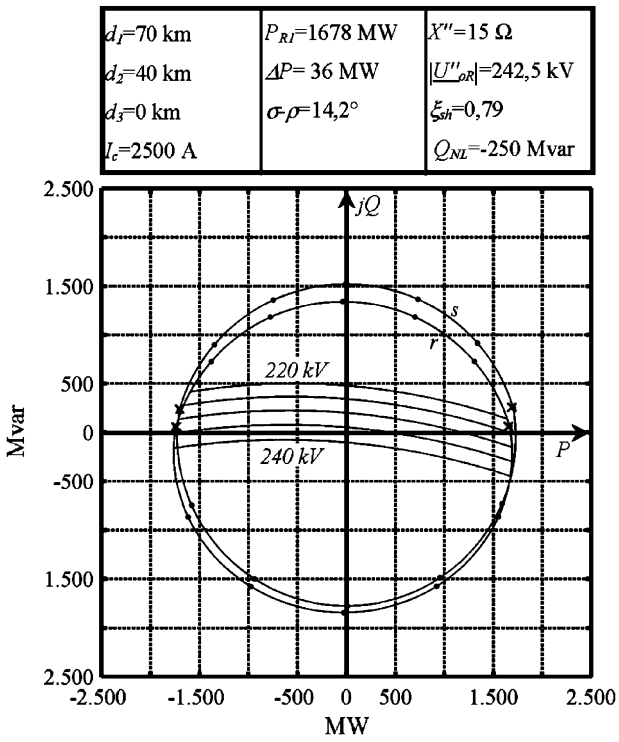

Fig. 13. Capability chart of specified mixed line.

It is also of note that the typical shape of capability charts with cusps at points × recurs chiefly each time there is a low compensated UGC as in [1].

In these cases (chiefly with high d_2 and low ξ_{sh}), the differences $\underline{S}_S - \underline{S}_R$ appear graphically very evident due to the strong reactive (capacitive) power absorbed by the cable. On the other hand, in the mixed lines (chiefly with high d_1, d_3 and ξ_{sh}) the reactive power absorbed by the overall link becomes of inductive nature (see Fig. 4 and Figs. 10–14), being prevalent the inductive demand of OHL.

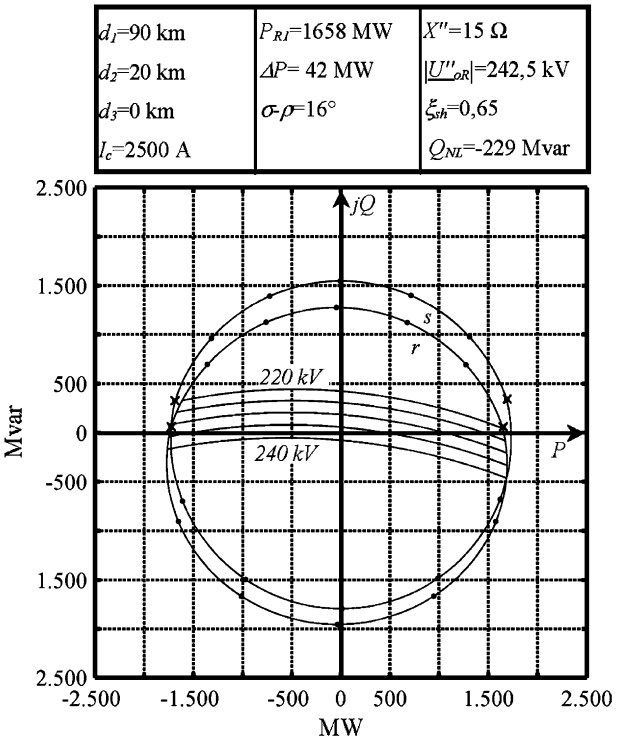

Fig. 12. Capability chart of specified mixed line.

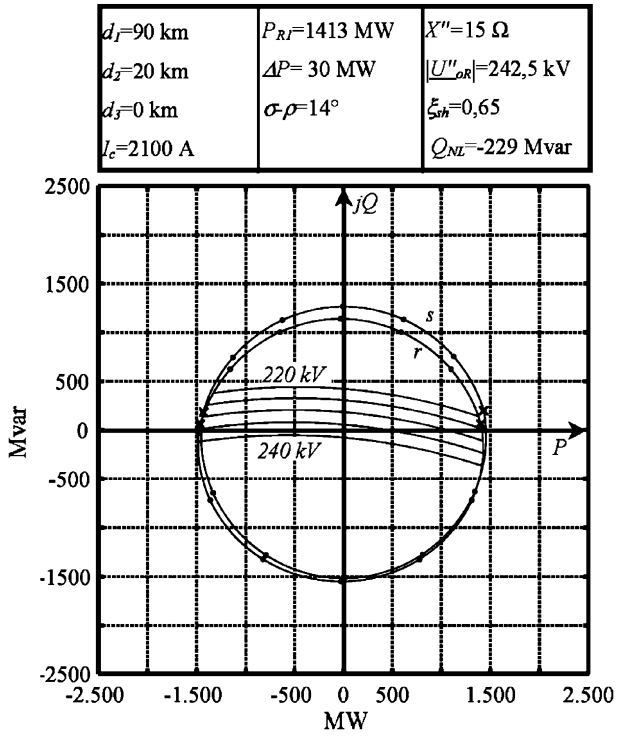

Fig. 14. Capability chart of specified mixed line.

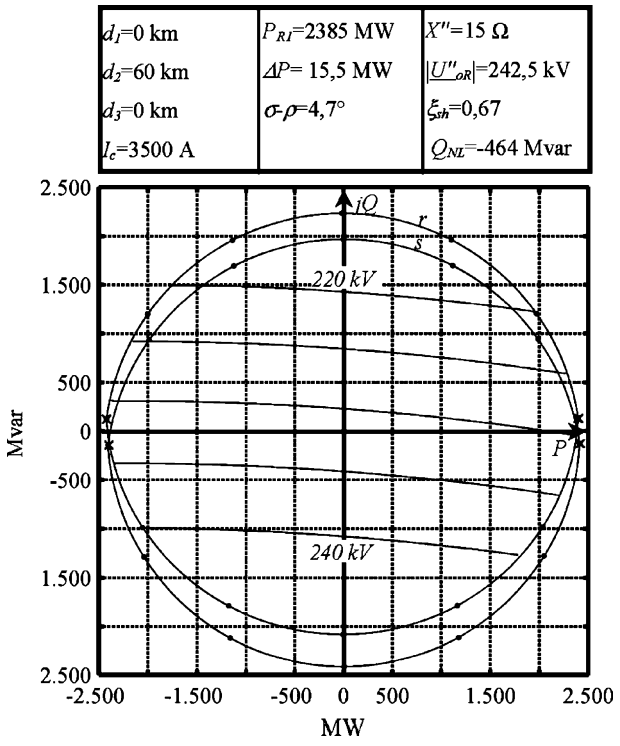

Fig. 15. Capability chart of double-circuit UGC.

8. "Receiving area" and "sending area" as intersections of sets

Once imposed (as in 1^ analysis) the phasors $I_K \angle 0 \equiv I_c$ and $\underline{U}_{oS}(\delta)$, if Eq. (22) is made explicit it is possible, being

$$\underline{N}_{R1} = \begin{vmatrix} \underline{A}_{R1} & \underline{B}_{R1} \\ \underline{C}_{R1} & \underline{D}_{R1} \end{vmatrix} \quad \begin{aligned} \underline{A}_{R1} &= \underline{D}_{123} - \underline{B}_{123}\underline{C}_{12}/\underline{A}_{12} \\ \underline{B}_{R1} &= -\underline{B}_{123}/\underline{A}_{12} \\ \underline{C}_{R1} &= -\underline{C}_{123} + \underline{A}_{123}\underline{C}_{12}/\underline{A}_{12} \\ \underline{D}_{R1} &= \underline{A}_{123}/\underline{A}_{12} \end{aligned},$$

to obtain the expression (27′)

$$\begin{aligned} \frac{\underline{S}_R(1^\wedge)}{3} &= [\underline{A}_{R1}\underline{U}_{oS} + \underline{B}_{R1}I_K] \cdot [\underline{C}_{R1}\underline{U}_{oS} + \underline{D}_{R1}I_K]^* \\ &= \underline{A}_{R1}\underline{C}^*_{R1}|\underline{U}_{oS}|^2 + \underline{B}_{R1}\underline{D}^*_{R1}I_K^2 + \underline{A}_{R1}\underline{D}^*_{R1}I_K\underline{U}_{oS}(\delta) \\ &\quad + \underline{B}_{R1}\underline{C}^*_{R1}I_K\underline{U}^*_{oS}(\delta). \end{aligned} \tag{27′}$$

Eq. (27′) gives the values of $\underline{S}_R(1^\wedge)/3$ for $\delta = 0 \div 2\pi$, without respecting for the limit I_c at node H.

Analogously once imposed (as in 2^ analysis) the phasors $I_H \angle 0 \equiv I_c$ and $\underline{U}_{oS}(\vartheta)$, if Eq. (23) is made explicit it is possible, being

$$\underline{N}_{R2} = \begin{vmatrix} \underline{A}_{R2} & \underline{B}_{R2} \\ \underline{C}_{R2} & \underline{D}_{R2} \end{vmatrix} \quad \begin{aligned} \underline{A}_{R2} &= \underline{D}_{123} - \underline{B}_{123}\underline{C}_1/\underline{A}_1 \\ \underline{B}_{R2} &= -\underline{B}_{123}/\underline{A}_1 \\ \underline{C}_{R2} &= -\underline{C}_{123} + \underline{A}_{123}\underline{C}_1/\underline{A}_1 \\ \underline{D}_{R2} &= \underline{A}_{123}/\underline{A}_1 \end{aligned},$$

to obtain the expression (28)

$$\begin{aligned} \frac{\underline{S}_R(2^\wedge)}{3} &= [\underline{A}_{R2}\underline{U}_{oS} + \underline{B}_{R2}I_H] \cdot [\underline{C}_{R2}\underline{U}_{oS} + \underline{D}_{R2}I_H]^* \\ &= \underline{A}_{R2}\underline{C}^*_{R2}|\underline{U}_{oS}|^2 + \underline{B}_{R2}\underline{D}^*_{R2}I_H^2 + \underline{A}_{R2}\underline{D}^*_{R2}I_H\underline{U}_{oS}(\vartheta) \\ &\quad + \underline{B}_{R2}\underline{C}^*_{R2}I_H\underline{U}^*_{oS}(\vartheta). \end{aligned} \tag{28}$$

Eq. (28) gives the values of $\underline{S}_R(2^\wedge)/3$ for $\vartheta = 0 \div 2\pi$, without respecting for the limit I_c at node K.

The simultaneous representation of both curves $\underline{S}_R(1^\wedge)$ and $\underline{S}_R(2^\wedge)$ which bound each other, allows drawing (once fixed I_c) the bound r of "receiving-end power area" (see Fig. 17).

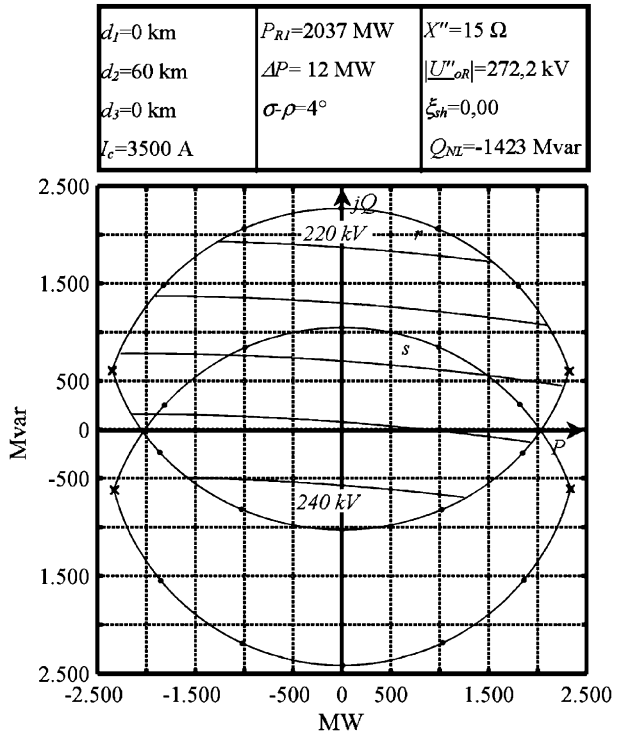

Fig. 16. Capability chart of double-circuit UGC.

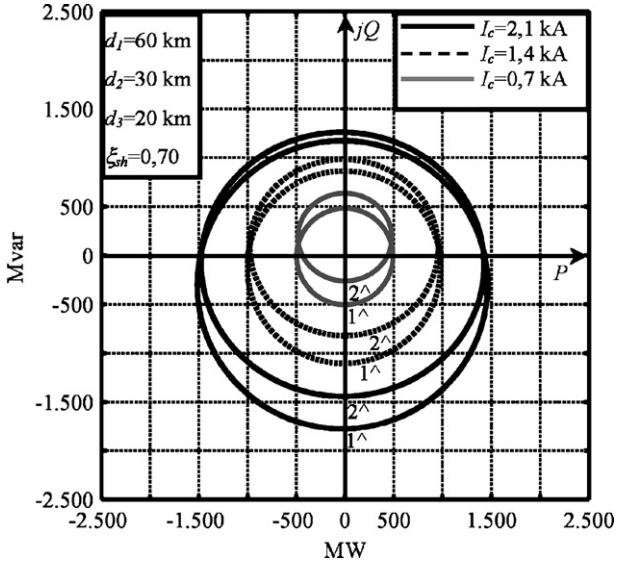

Fig. 17. Delimiting the receiving areas by means Eqs. (27) and (28).

With similar procedure, by developing Eqs. (8) and (17), it is possible to have Eqs. (29) and (30)

$$\frac{\underline{S}_S}{3}(1^{\wedge}) = \underline{U}_{oS}[\underline{C}_{S1}\underline{U}_{oS} + \underline{D}_{S1}I_K]^* = \underline{C}^*_{S1}|\underline{U}_{oS}|^2 + I_K\underline{D}^*_{S1}\underline{U}_{oS}(\delta) \quad (29)$$

$$\frac{\underline{S}_S}{3}(2^{\wedge}) = \underline{U}_{oS}[\underline{C}_{S2}\underline{U}_{oS} + \underline{D}_{S2}I_H]^* = \underline{C}^*_{S2}|\underline{U}_{oS}|^2 + I_H\underline{D}^*_{S2}\underline{U}_{oS}(\vartheta) \quad (30)$$

so that, by means of $\underline{S}_S(1^{\wedge})$ and $\underline{S}_S(2^{\wedge})$, the bound s of "sending-end power area" can be drawn. Eqs. (29) and (30) give circumferences, whereas Eqs. (27′) and (28) give ellipses with low eccentricity since beyond the third term with $\underline{U}_{oS}$ there is a forth term (generally slight) with the complex conjugate $\underline{U}^*_{oS}$. This kind of approach, which determines the sending-end power area and receiving-end power area as *intersection of sets*, can become very useful to draw the capability charts of a line with different (for location and magnitude) ampacity constraints.

9. Conclusions

The cable lines together with mixed ones can lessen sensibly many route problems by virtue of their adaptability in the territory and have become a recurring topic in the technical literature [5,6].

The authors have already presented comprehensive algorithms to deeply analyse the transmission performances of UGC. In this paper, the method has been further developed and extended to take into account mixed lines composed of overhead and cable lines. This has been performed by means of capability charts which highlights at quick glance the whole field of transmissible complex power compatibly with the assumed constraints for both current and voltage and are enhanced with other power transmission features, which result very useful to evaluate the composite link operation.

This gives a meaningful contribution to both the grid planning and operation.

The CPU-time to compute a capability chart is about 4 s (PC Pentium 2.8 GHz, RAM 1048 MB). The procedure is versatile as well since it can be easily applied to more simple mixed lines ($d_1 = 0$ or $d_3 = 0$), to only cable line ($d_1 = 0 = d_3$) and to other configurations.

The paper is also a powerful guide to choose the shunt compensation degree of UGC in order to limit the overvoltages in case of line energization. Although the hypothesis of uniformly distributed compensation has been adopted, the method is easily applicable to lumped one (at each ends or also at intermediate locations).

Appendix A

For each section ① , ② and ③ the corresponding classical transmission matrices must be calculated as in (A1)

$$\underline{\boldsymbol{M}}_1 = \begin{bmatrix} \underline{A}_1 & \underline{B}_1 \\ \underline{C}_1 & \underline{D}_1 \end{bmatrix}; \quad \underline{\boldsymbol{M}}_2 = \begin{bmatrix} \underline{A}_2 & \underline{B}_2 \\ \underline{C}_2 & \underline{D}_2 \end{bmatrix}; \quad \underline{\boldsymbol{M}}_3 = \begin{bmatrix} \underline{A}_3 & \underline{B}_3 \\ \underline{C}_3 & \underline{D}_3 \end{bmatrix}. \quad (A1)$$

$$\underline{\boldsymbol{M}}_\xi = \begin{bmatrix} 1 & 0 \\ \underline{Y}_\xi & 1 \end{bmatrix} \quad (A5)$$

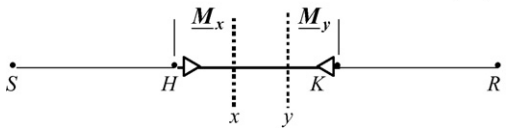

Fig. A1. Checking the regimes along UGC by means of (A4′) and (A4″).

They depend upon the line parameters and line length d_1, d_2, d_3. In the hypothesis of uniformly distributed compensation in UGC ② , the elements $\underline{A}_2$, $\underline{B}_2$, $\underline{C}_2$, are computed as in [1]. The equivalent cascade matrices are given

$$\underline{\boldsymbol{M}}_{123} = \underline{\boldsymbol{M}}_1\underline{\boldsymbol{M}}_2\underline{\boldsymbol{M}}_3 = \begin{bmatrix} \underline{A}_{123} & \underline{B}_{123} \\ \underline{C}_{123} & \underline{D}_{123} \end{bmatrix}; \quad \underline{\boldsymbol{M}}_{12} = \underline{\boldsymbol{M}}_1\underline{\boldsymbol{M}}_2 = \begin{bmatrix} \underline{A}_{12} & \underline{B}_{12} \\ \underline{C}_{12} & \underline{D}_{12} \end{bmatrix} \quad (A2)$$

Note that generally even if $\underline{D}_1 \equiv \underline{A}_1$, $\underline{D}_2 \equiv \underline{A}_2$, $\underline{D}_3 \equiv \underline{A}_3$, the same is not valid for the cascade matrix elements i.e. $\underline{D}_{12} \neq \underline{A}_{12}$ and $\underline{D}_{123} \neq \underline{A}_{123}$. The inverse matrices are given in the following (A3) relation (if it is valid the reciprocity principium which yields $\underline{A}_i\underline{D}_i - \underline{B}_i\underline{C}_i = 1$).

$$\underline{\boldsymbol{M}}_i = \begin{bmatrix} \underline{A}_i & \underline{B}_i \\ \underline{C}_i & \underline{D}_i \end{bmatrix} \qquad \underline{\boldsymbol{M}}_i^{-1} = \begin{bmatrix} \underline{D}_i & -\underline{B}_i \\ -\underline{C}_i & \underline{A}_i \end{bmatrix} \quad (A3)$$

The check (in $1^{\wedge}$ and $2^{\wedge}$ analysis) along UGC (see Fig. A1) can be performed by means of (A4′) and (A4″), by using $\underline{\boldsymbol{v}}_{\boldsymbol{HH(K)}}$ from (9) and $\underline{\boldsymbol{v}}_{\boldsymbol{KK(H)}}$ from (18):

$$(1^{\wedge}) \quad \underline{\boldsymbol{v}}_{\boldsymbol{xx}} = \underline{\boldsymbol{M}}_{\boldsymbol{x}}^{-1} \cdot \underline{\boldsymbol{v}}_{\boldsymbol{HH(K)}} \quad (A4')$$

$$(2^{\wedge}) \quad \underline{\boldsymbol{v}}_{\boldsymbol{yy}} = \underline{\boldsymbol{M}}_{\boldsymbol{y}} \cdot \underline{\boldsymbol{v}}_{\boldsymbol{KK(H)}} \quad (A4'')$$

It worth noting that each installation of three single-pole shunt reactors, with admittance $\underline{Y}_\xi$, requires the cascade insertion (in the suitable position) of the relevant matrix $\underline{\boldsymbol{M}}_\xi$:

$$\underline{\boldsymbol{M}}_\xi = \begin{bmatrix} 1 & 0 \\ \underline{Y}_\xi & 1 \end{bmatrix} \quad (A5)$$

Appendix B. List of symbols

ac	alternating current
$\underline{A}_i, \underline{B}_i, \underline{C}_i, \underline{D}_i$	transmission coefficients of ith section
d_1	length of section ① (OHL)
d_2	length of section ② (UGC)
d_3	length of section ③ (OHL)
EHV	extra high voltage
I_a	ampacity
I_c	chosen current constraint
$\underline{M}_i$	transmission matrix of ith section
$\underline{M}_{12}$	cascade matrix of $\underline{M}_1$ and $\underline{M}_2$
$\underline{M}_{123}$	cascade matrix of $\underline{M}_1$, $\underline{M}_2$ and $\underline{M}_3$
OHL	overhead line
Q_{NL}	capacitive power absorbed by mixed line at no-load
U	phase-to-phase voltage
U_o	phase-to-earth voltage

U_{oc} chosen phase-to-earth voltage level at node S
UGC underground cable line
$\underline{W}$ complex number
$\underline{W}^*$ complex conjugate
XLPE cross-linked polyethylene
$\underline{Z}''$; (X'') short-circuit subtransient impedance; (reactance)
ξ_{sh} shunt compensation degree $(0 \div 1)$ in the section ② (UGC)

Subscripts
H intermediate end
K intermediate end
R receiving-end
S sending-end
o phase-to-earth

References

[1] R. Benato, A. Paolucci, Operating capability of long ac EHV transmission cables, Electric Power Syst. Res. 75 (1) (2005) 17–27.
[2] R. Benato, Multiconductor analysis of underground power transmission systems: EHV Cables, Electric Power Syst.Res., submitted for publication.
[3] R. Benato, A. Paolucci, Flussi di potenza in sistemi multiconduttore a struttura dissimmetrica. Un programma per PC, L'Energia Elettrica 77 (6) (2000) 43–53.
[4] British Electricity International, Modern Power Station Practice, EHV Transmission, vol. K, third ed., Pergamon Press, Oxford, 1991 (Chapter 9, Section 3.3, Control of switching surges).
[5] R. Rendina, A. Posati, M. Rebolini, G. Bruno, F. Bocchi, M. Marelli, A. Orini, The new Turbigo-Rho 380 kV transmission line: an example of the use of underground XLPE cables in a meshed transmission grid, in: CIGRÉ, 2006, p. B1-301.
[6] F.M. Gatta, S. Lauria, Very long EHV cables and mixed overhead-cable lines. Steady-state operation, in: Proceedings of IEEE St. Petersburg Power Tech'05 Conference, St. Petersburg, Russia, June 27–30, 2005.

Roberto Benato was born in Venezia, Italy, in 1970. He received the DrIng Degree in electrical engineering from the University of Padova in 1995 and PhD in power systems analysis in 1999. In 2002, he was appointed as assistant professor in the Power System Group at the Department of Electrical Engineering at Padova University. His main fields of research are multiconductor analysis, EHV–HV transmission lines and advanced matricial techniques for the static and dynamic power system analysis. He is member of CIGRÉ WG B1.08 "Cable systems in multipurpose or shared structures", secretary of CIGRÉ JWG B3-B1.09 "Application of Long High Capacity Gas Insulated Lines in Structures" and member of IEEE PES Substations Committee. He is also a member of IEEE and Italian AEIT.

Antonio Paolucci was born in Padova, Italy, in 1924. He received the DrIng Degree in electrical engineering from the University of Padova in 1950. He joined the department of electrical engineering of the University of Padova in 1952 where he was assistant and later associate professor. From 1973 to 2000 he has been full professor of power systems analysis. At present, he participates in Power System Research Group of University of Padova. He is a member of AEIT.